Supporting information for

Unidirectional broadband light emission from supported plasmonic nanowires

by Timur Shegai, Vladimir D. Miljković, Kui Bao, Hongxing Xu, Peter Nordlander, Peter Johansson, and Mikael Käll

S1 Estimation of wire diameter from optical contrast

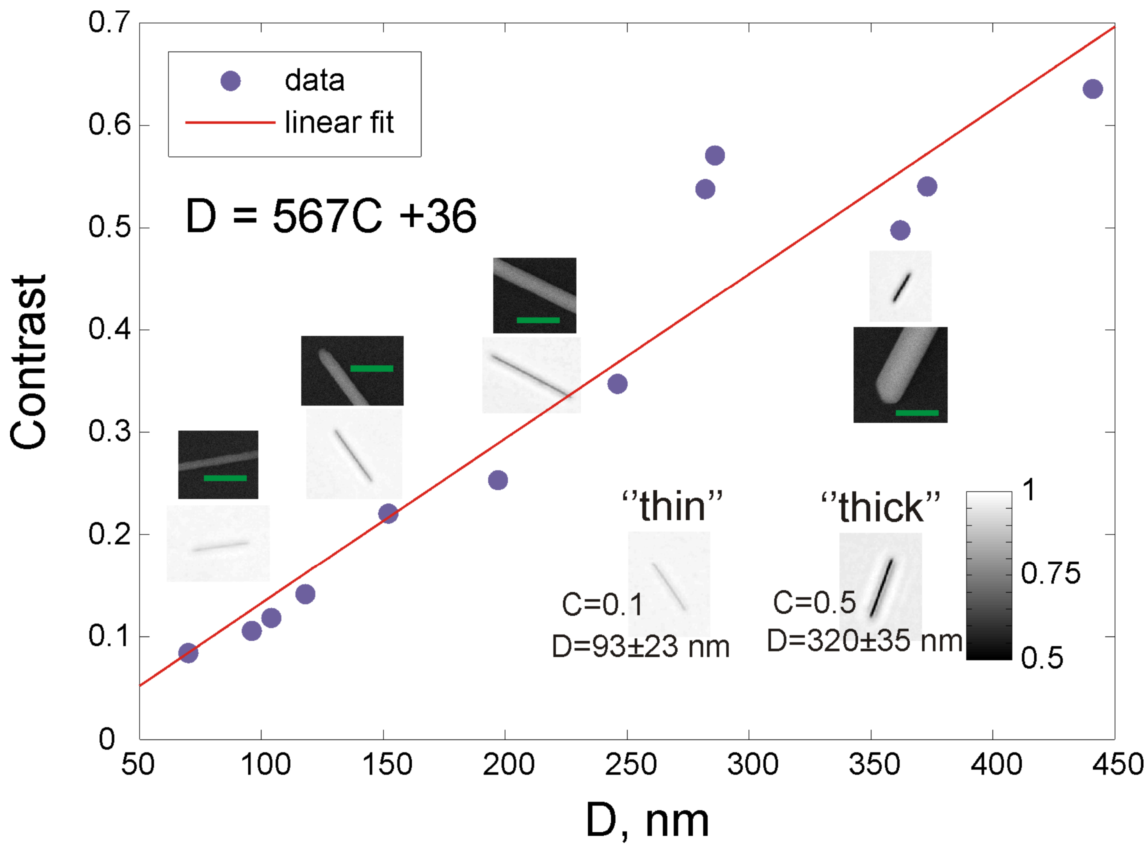

Figure S1. Optical contrast versus wire diameter. Optical images of nanowires were obtained using wide-field optical transmission microscopy (gray scale in 0.5-1 range) and their diameters were measured using low vacuum SEM (green bar = 500 nm). The data is well fit by a linear curve and the diameter can be estimated by a D=567(±55)·C+36(±22) formula, where, D is the diameter in nm and C is contrast, defined as $(1\text{-}I_{min})$. The diameters of the 'thin' and 'thick' wires presented in the main text were estimated to be 93±23 nm and 320±35 nm, respectively.

S2 Dipole near interface

The problem of light emission from a dipole located near a flat dielectric interface has a long history [S1-S3]. The radiated intensity can be found from the far-field properties of the dyadic Green's function. Figure S2 shows calculated Fourier images, $I(\theta, \phi)$ in the notation of Ref. [S3], for a single dipole as a function of its orientation and distance to the interface. Note that (i) the light emission is concentrated near the critical angle θ_c; (ii) the forbidden light ($\theta > \theta_c$) decreases rapidly in intensity as the dipole-interface distance grows and (iii) the dipole orientation strongly affects the radiation pattern. However, none of the patterns exhibit unidirectional emission.

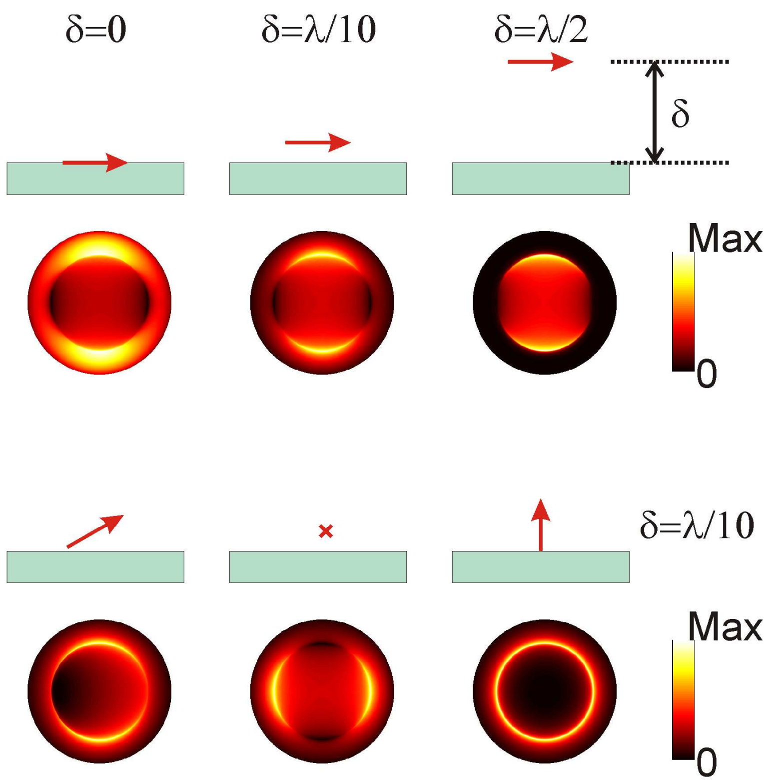

Figure S2. Fourier images of a point dipole source located at various distances and with various orientations with respect to an air-glass interface. The dipole radiates at λ=633 nm. The top row shows dipoles oriented parallel to the interface but at different distances from the interface. The bottom row shows dipoles at a distance of λ/10 from the interface but oriented differently. Two distinct lobes at the critical angle appear in accordance with the dipole polarization. The outer radius of the Fourier plane corresponds to NA=1.49.

S3 Chain of dipoles near an interface

In contrast to the single dipole patterns, Figure S3 shows strongly directional radiation. These are Fourier images obtained when a chain of 10 equally spaced identical dipoles oscillate with the same frequency but different phases to mimic a propagating plasmon. The dipole moments are thus modulated by a phase factor $\exp(ik_{spp}x_i)$, where $k_{spp} = 2\pi/\lambda_{spp}$ corresponds to the plasmon wave vector and x_i is the dipole position along the chain. The intensity I_N resulting from $N = 10$ dipoles is then given by the single-dipole intensity $I(\theta, \phi)$ modulated by a structure factor $|S(\theta, \phi)|^2$

$$I_N(\theta, \phi) = |S(\theta, \phi)|^2 \, I(\theta, \phi), \qquad \text{(S1)}$$

where

$$S(\theta,\phi) = \sum_{i=1}^{N} e^{i(k_{spp} - nk\sin\theta\cos\phi)x_i} \;, \qquad \text{(S2)}$$

n is the glass refractive index, and $k = \omega/c$. The fringes seen in all images in Figure S3 result from the fact that S only depends on the x coordinate in the Fourier plane. At the same time, one can also see traces of the circular patterns of Figure S2 originating from $I(\theta, \phi)$. The structure factor is the main cause for all the primary maxima seen in Figure S3. For λ_{spp} = 570nm the primary maximum of $|S|^2$ due to constructive interference between all the dipoles runs through the forbidden part of the Fourier plane, $\theta_c < \theta < 90^0$. For λ_{spp} = 400nm the primary maximum of $|S|^2$ falls further to the right in the Fourier image, in the part corresponding to evanescent waves, outside $\theta = 90^0$. But since the chain of dipoles is finite, this interference fringe has a tail at $\theta < 90^0$ that gives rise to the maxima in the Fourier images in this case.

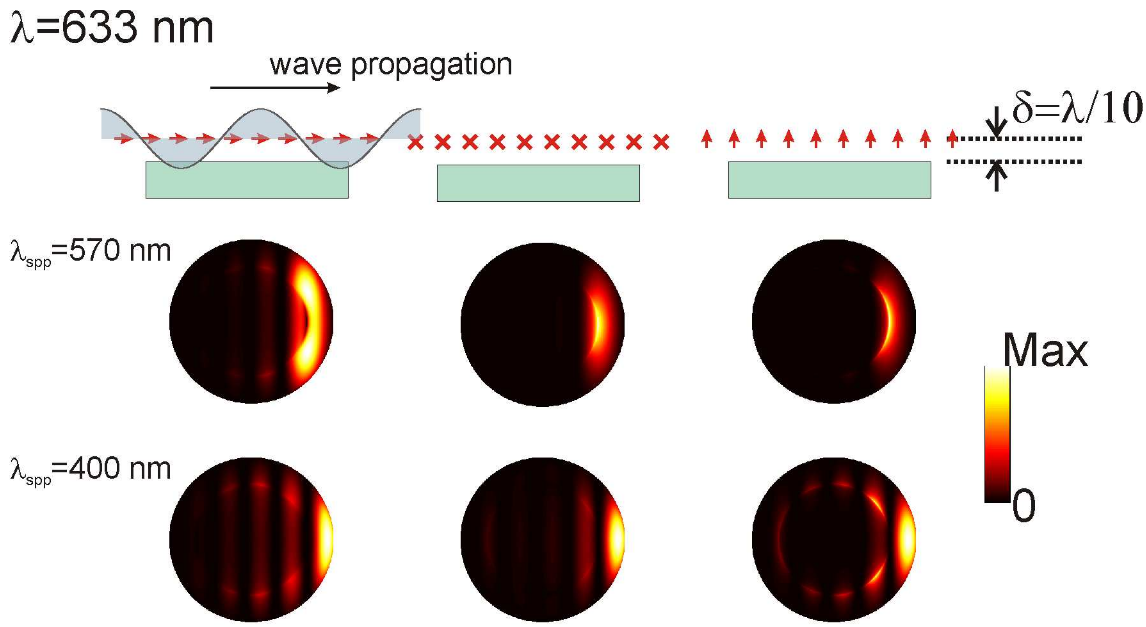

Figure S3. Fourier images of a chain of dipoles (N = 10) in air at a distance of λ/10 above a glass interface at λ=633 nm. The phase retardation between the dipoles is defined according to a surface plasmon wavelength of λ_{SPP}=570 nm for the top row and λ_{SPP}=400 nm for the bottom row. These plasmon wavelengths correspond to the thick and thin wires cases from the infinite metal cylinder model (see Fig. 3 (c, d) and paragraph S5 below). The length of the dipole chain is taken to be 1 micron. Three different dipole orientations are shown.

S4 Aperture translation and polarization imaging

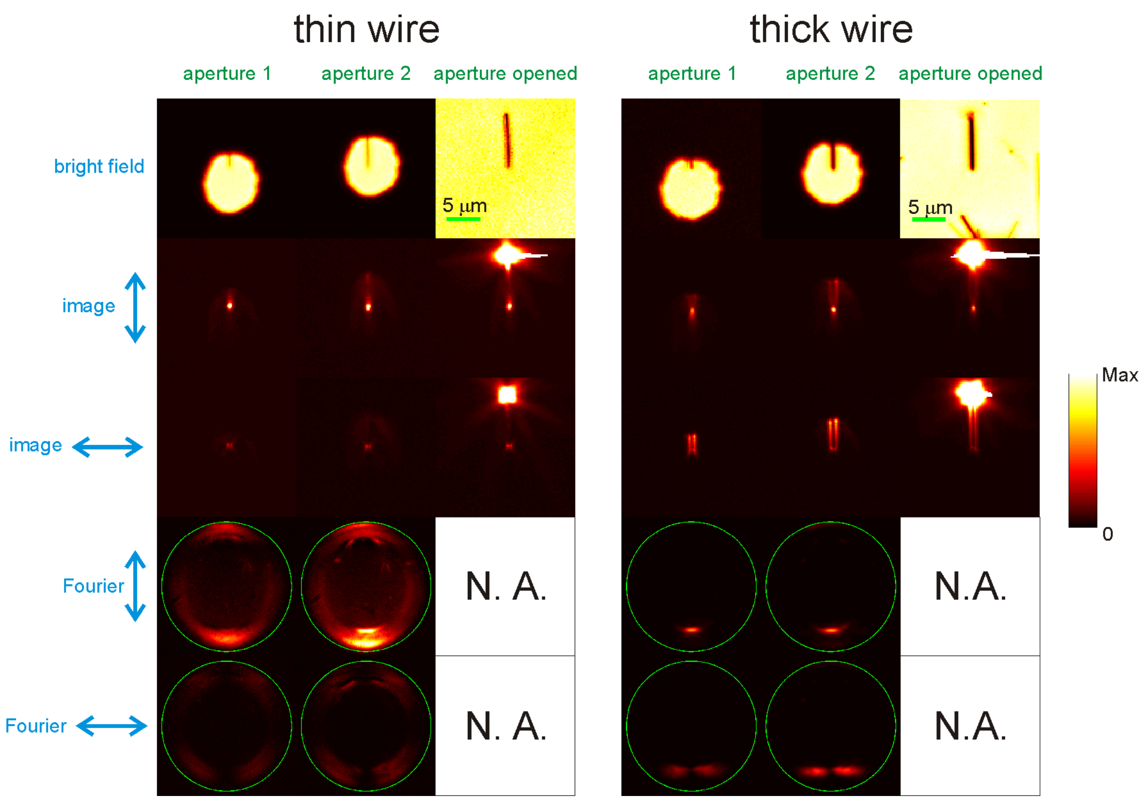

Figure S4. Demonstration that the directional light comes from the length of the wire rather than from the tip for a thick and a thin wire case. Top row shows bright field images with two positions of the aperture along the wires and a fully opened aperture. The second and third row of images show emission polarized parallel and perpendicular to the wires when they are excited by focused unpolarized white light at the input (top) end. The two lower rows of images show the corresponding Fourier images. All images are shown in the same intensity scale.

S5 Fabry-Perot resonator and infinite metal cylinder model.

In order to retrieve the dispersion relation for metal wires from the spectral information, we utilize the Fabry-Perot resonator model according to ref [S4-S5]. The maxima in the emission spectra correspond to constructive interference between forward and backwards propagating plasmons, meaning that an integer number of half plasmon wavelengths fit in a resonator of length L [S4-S5]. Thus, the plasmon wavevector k_{spp} is given by:

$$k_{spp} = \frac{\pi n - \phi_{ref}}{L} \approx \frac{\pi n}{L} \tag{S3}$$

where n is the mode order and ϕ_{ref} is the phase shift upon reflection at the wire ends. The phase shift can be neglected in the present case because n>>1, but is important for short wires and/or for very long wavelengths [S6-S8]. Note that both even and odd resonances are excited in the present case as the symmetry is broken by the oblique illumination (the wave vector thus changes by $\Delta k_{spp} \approx \pi / L$ between successive spectral maxima). Since the length L of a wire that produces a certain standing wave pattern is known, the dispersion relation can be reconstructed if we can specify n, see Figure S5 for a graphical illustration. One can find n with a quite high degree of certainty if we first note that the slope of the dispersion curve, i.e the group velocity, at a certain frequency is independent of k due to Eq. S3 (i.e. $v_g \approx L/_{\pi} \Delta\omega$). Specifying n thus corresponds to translating the dispersion curve along the k-axis such that it approaches ω=0 in the limit $k_{spp}=0$ for all dielectric environments measured. The choice of n is further restricted if we note that the experimental dispersion curve for the uniform surrounding (oil/glass) should match the plasmon dispersion for an infinite silver cylinder with the same diameter reasonably well. The latter is known from wave guide theory and the propagating TM0 modes are given by [9-10]:

$$\frac{\varepsilon}{\kappa_1 R}\frac{J_1(\kappa_1 R)}{J_0(\kappa_1 R)} - \frac{\varepsilon_d}{\kappa_2 R}\frac{H_1^{(1)}(\kappa_2 R)}{H_0^{(1)}(\kappa_2 R)} = 0 \tag{S4}$$

where J_n and $H_n^{(1)}$ are cylindrical Bessel and Hankel functions, $\kappa_{1(2)} = k_0\sqrt{\varepsilon_{(d)} - (k_{spp}/k_0)^2}$, ε is real part of the dispersive dielectric constant of silver, ε_d is the dielectric constant of the environment, k_0 is the vacuum wave vector and R is the wire radius. By solving (S4) numerically with respect to k_{spp}, using experimental values for $\varepsilon(\lambda)$ [S11], one obtains a dispersion relation for the wire. In Figure 3(c-d) in the main text, the solution for the D=80 and D=320 nm silver wires is shown in various homogeneous media. The agreement between experimental and simulated dispersion curves is apparent.

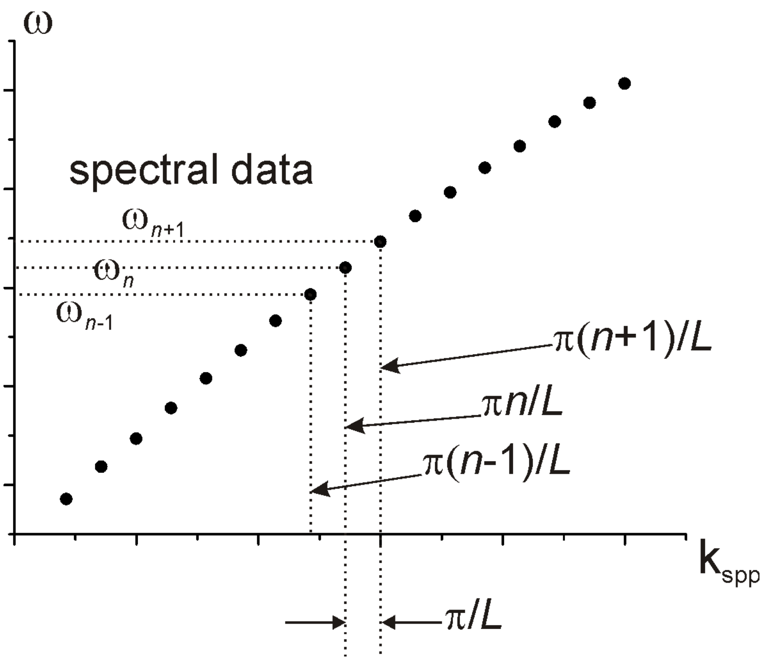

Figure S5. Sketch of the methodology for retrieving the dispersion relation curve from the standing wave pattern.

Supporting information references:

S1 Lukosz, W. & Kunz, R. E. Light-emission by magnetic and electric dipoles close to a plane interface. 1. Total radiated power. *Journal of the Optical Society of America* **67**, 1607-1615, (1977).

S2 Lukosz, W. & Kunz, R. E. Light emission by magnetic and electric dipoles close to a plane dielectric interface. 2. Radiation patterns of perpendicular oriented dipoles. *Journal of the Optical Society of America* **67**, 1615-1619, (1977).

S3 Lieb, M. A., Zavislan, J. M. & Novotny, L. Single-molecule orientations determined by direct emission pattern imaging. *Journal of the Optical Society of America B-Optical Physics* **21**, 1210-1215, (2004).

S4 Ditlbacher, H. *et al.* Silver nanowires as surface plasmon resonators. *Physical Review Letters* **95**, 257403, (2005).

S5 Dorfmuller, J. *et al.* Fabry-Perot Resonances in One-Dimensional Plasmonic Nanostructures. *Nano Letters* **9**, 2372-2377, (2009).

S6 Barnard, E. S., White, J. S., Chandran, A. & Brongersma, M. L. Spectral properties of plasmonic resonator antennas. *Optics Express* **16**, 16529-16537, (2008).

S7 Sondergaard, T. & Bozhevolnyi, S. I. Strip and gap plasmon polariton optical resonators. *Physica Status Solidi B-Basic Solid State Physics* **245**, 9-19, (2008).

S8 Sondergaard, T., Beermann, J., Boltasseva, A. & Bozhevolnyi, S. I. Slow-plasmon resonant-nanostrip antennas: Analysis and demonstration. *Physical Review B* **77**, 115420, (2008).

S9 Novotny, L. Effective wavelength scaling for optical antennas. *Physical Review Letters* **98**, (2007).

S10 Novotny, L. & Hafner, C. Light propagation in a cylindrical wave-guide with a complex, metallic, dielectric function. *Physical Review E* **50**, 4094-4106, (1994).

S11 Johnson, P. B. & Christy, R. W. Optical-constants of noble-metals. *Physical Review B* **6**, 4370-4379, (1972).